Ultimate Limit State Fragility of Offshore Wind Turbines on Monopile Foundations

David Wilkie[a] and Carmine Galasso[a]

[a] Department of Civil Environmental & Geomatic Engineering, University College London, UK.

Abstract: Assessing the risk posed by extreme natural events to the failure of offshore wind turbines (OWTs) is a challenging task. Highly stochastic environmental conditions represent the main source of variable loading; consequently, a high level of uncertainty is associated with assessing the structural demand on OWT structures. However, failure of any of the primary structural components implies both complete loss of the OWT and loss of earnings associated with production stoppage (i.e., business interruption).

In this paper, we propose the use of the Catastrophe (CAT) Risk Modelling approach to assess the structural risk posed by extreme weather conditions to OWTs. To help achieving this, we develop fragility curves – a crucial element of any CAT models – for OWTs on monopile foundations. Fragility functions express the likelihood of different levels of damage (or damage states) sustained by a given asset over a range of hazard intensities. We compare the effect of modelling and analysis decisions on the fragility curves, highlighting how different procedures could affect the estimated probability of failure. We apply the proposed framework to two case-study locations, one in the Baltic Sea and one in the North Sea.

1 Introduction

The offshore wind industry has grown to the point where it supplies 11.03GW of electricity within Europe, with a further 26.4GW of projects approved [1]. Approximately 80% of the offshore wind turbines (OWTs) generating this power are on monopile foundations. One of the key elements in designing offshore structures - or in assessing existing ones - is the estimation of the wind and wave loading likely to be encountered during their life time. The design and assessment of OWTs is currently based on deterministic (or semi-probabilistic) and prescriptive approaches, employing safety factors to be applied to deterministic design quantities (i.e., load and resistance) and notional return periods for the load conditions to be considered in the design. There are uncertainties associated with the calculation of structural capacity (e.g., geometry, materials) as well as bias in modelling assumptions. These uncertainties become particularly significant when considering extreme weather conditions which are intrinsically more difficult to predict. Poor characterisation of these uncertainties could lead to either too conservative designs or unsafe ones, with potentially catastrophic losses. This poses significant technical challenges but can also severely increase the cost of financing offshore projects.

A framework based on Catastrophe (CAT) risk modelling is proposed here to assess structural and non-structural risk associated with OWTs exposed to European extra-tropical cyclones (ETCs; i.e., winter storms). The proposed approach can be used to test innovative design strategies – extending

performance-based engineering frameworks (also accounting for combined hazards); to devise efficient and targeted asset management; and to develop resilience-enhancing solutions for combined wave and wind hazards (e.g., based on structural health monitoring and structural control). This can help to reduce overall costs and ultimately reduce the levelized electricity cost for offshore wind farms (OWFs). Figure 1 shows the basic structure of a CAT modelling approach which has been adapted here for application to OWFs. The overall framework can be decomposed into a series of sequential components [2]: exposure (information about asset location, construction details and replacement values), hazard (reliable estimation of relevant hazard intensities and their recurrence periods), structural analysis (reliable estimation of engineering demand parameters, or EDPs, given hazard intensities), and fragility (reliable estimation of damage and downtime given hazard intensities). The synthesis of such a framework (loss) provides many valuable decision-making and management metrics, for example, the average annual loss of an OWF or the association of total loss magnitudes with recurrence periods.

Fragility functions, quantifying the probability of reaching certain limit-states, or performance levels (e.g., minor damage to complete structural collapse), given events of different intensities, are fundamental tools in any CAT model. Damage-to-loss functions can then be used to convert the damage estimates (from fragility) to loss estimates. Very few examples of such functions exist, and no established guidance exist for calculating them.

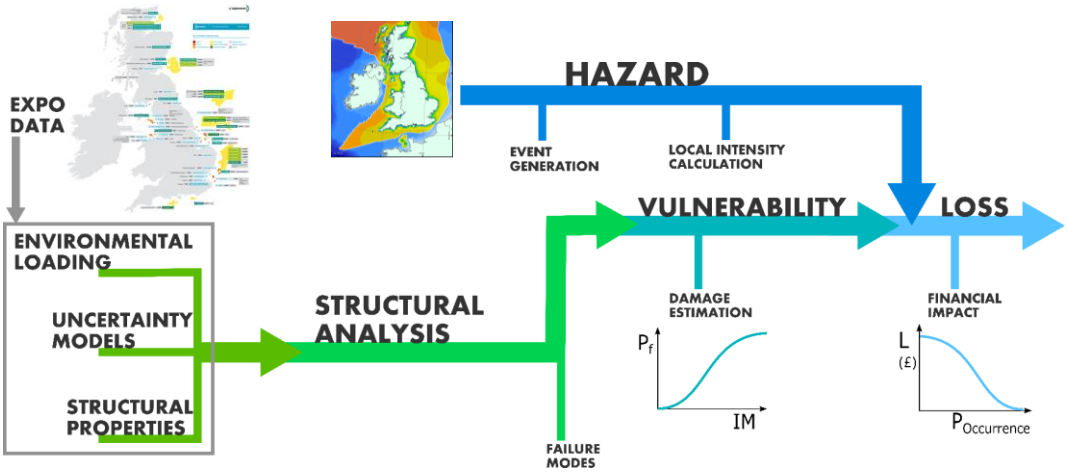

Figure 1: Catastrophe modelling framework applied to an OWF.

In particular, analytical (i.e., structural simulation-based) fragility is commonly used, especially in earthquake engineering, where such curves have been developed for a range of civil engineering structures due to the lack of loss/damage statistics from past events. In wind engineering, Sorensen [3] developed a limit state for failure of onshore turbine towers and proposed a range of random variables to capture uncertainty in modelling assumptions. Assessment of OWT is more challenging because they are exposed to both wind and wave loading. The fragility of OWT on jackets was investigated by Wei et al [4], who developed a performance-based assessment using results from nonlinear static analysis to calculate the extreme response followed by Monte Carlo sampling to associate a probability of failure with different return periods. The result was fragility curves based on damage, first yield, and collapse limit states using the jacket base shear as an EDP. Similarly, fragility of OWT on monopile foundations exposed to wind, wave and earthquake hazards was investigated by Mardfekri [5]. Fragility curves investigated wind speed and wave height independently as the focus was quantifying simulation bias using high-performance computing. Techniques for assessing wind- and wave- induced demand on OWTs include Incremental Wind Wave

Analysis (IWWA) [6] where the structural response to progressively increasing waves heights and wind speeds is calculated. In IWWA, wind and wave conditions are coupled using mean return period (MRP) or a joint probability distribution and the output is the structural response to increasingly rare environmental conditions. The existing implementation of the IWWA is based on non-linear static analysis [6]. Due to the larger flexibility of OWT on monopiles and the need to capture rotor dynamics, we propose the use of IWWA [6] with coupled time-history analysis; we also consider additional random variables to represent modelling uncertainty. Additionally, there has been little research comparing the effect of different modelling and analysis assumptions on the fragility of an OWT. The work referenced has continually identified the low probability of failure associated with OWT structures exposed to normal (non-hurricane) conditions, therefore there is benefit to investigating the lower tail of the fragility curve. Plain Monte Carlo techniques are poor in this region and alternative, more advanced techniques may be more appropriate.
The paper investigates the sensitivity of fragility functions to different modelling and analysis decisions. We develop fragility functions for a reference OWT support structure at two different OWF sites. The influence of analysis length, extreme load calculation, definition of limit state function and the influence of including uncertainties is discussed. In addition, we investigate improving prediction of the lower tail of the fragility curve using the subset simulation [7] technique.

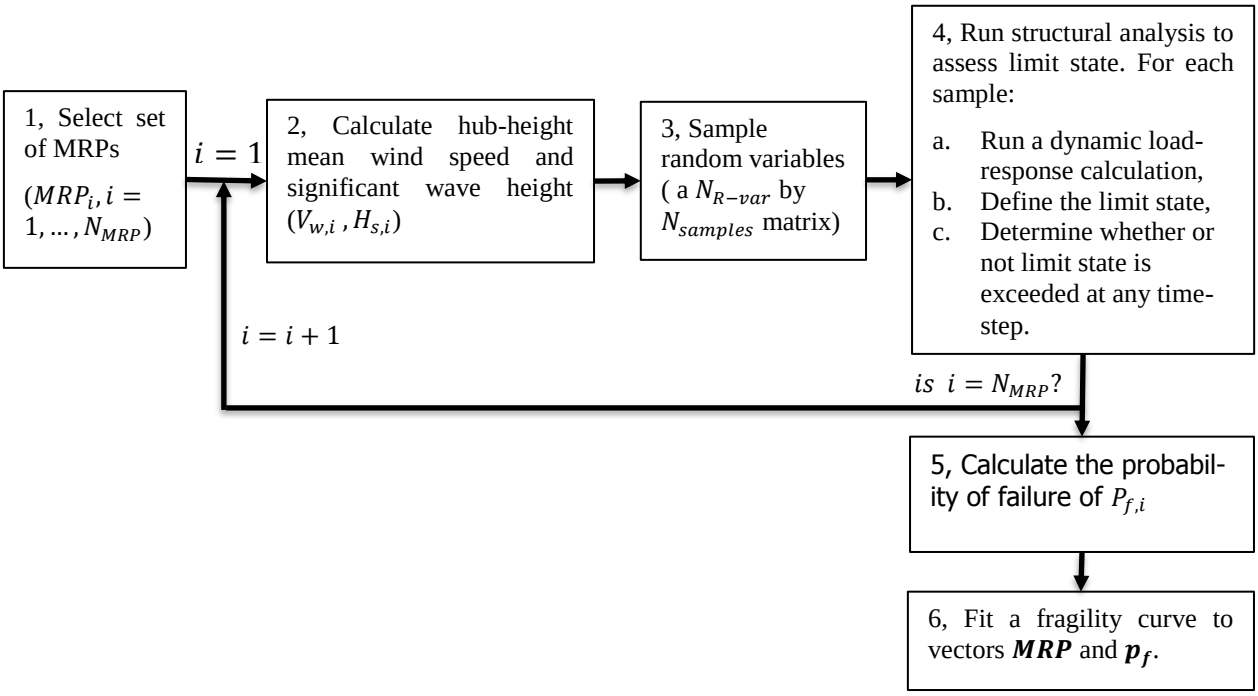

Figure 2: Flowchart describing the fragility calculation procedure.

2 Fragility Calculations

2.1 Methodology

The fragility calculation procedure is comprised of the six steps described on the flowchart in Figure 2. The details required to implement the calculation are discussed in Section 2.3. This process allows a structural analysis package, such as Fatigue Aerodynamics Structures and Turbulence (FAST) to be incorporated within the fragility calculation. It is also sufficiently general to encompass most forms of simulation technique, in this paper we apply both plain Monte Carlo and subset

simulation [7]. The 3rd and 4th steps of the fragility calculation are different when using subset simulation as this technique is based on generating values of each input sample adaptively during the reliability calculation, therefore they cannot be generated in advance. Separately two techniques are used to compute EDP values used in the reliability calculation:

Non-parametric - EDPs are calculated by running structural analysis directly using the desired environmental conditions as inputs. This means we directly simulate a broad range of environmental conditions and each sample used in the fragility calculation corresponds directly to the output from a structural analysis runs. At higher MRP the analysis might start to produce physically meaningless results, for example waves that have troughs lower than the seabed. As a result, the envelope of environmental conditions directly assessed has been limited to a maximum MRP of 10^9.

Parametric - A second approach to EDP calculation attempted to alleviate the problem of having a limited number of samples at each MRP by fitting a conditional distribution of EDP given a MRP to output from structural analysis and substituting the resulting distribution into the limit state equation. A Generalised Extreme Value (GEV), Weibull and Lognormal distribution were also tested but the GEV was found have the consistently highest log-likelihood. This made it faster to recalculate the limit state, allowing a larger sample sizes to be generated.

2.2 Case Study Site and Environment

Two sites were investigated in this study because of their contrasting environmental conditions: Ijmuiden [8], located in the Netherlands, and Krieger's Flak [9], located in Denmark. Ijmuiden has 22 years' worth of wind and wave measurements [8], and distributions representing the occurrence of different mean wind speeds and significant wave heights [10] have been published [8]. Krieger's Flak has 10 years' metocean data and the full set of hourly wind and wave recordings were published, a 3-parameter Weibull distribution was fit to estimate the probability of different extreme wind and wave results. The environmental conditions associated with a set of different MRP are plotted on Figure 3 (left) and all data has a 10-minute averaging period. Intensity levels were simplified by combining the wind and wave conditions into a single metric – the MRP, this approach is conservative [6] but simplified the analysis substantially. Both sites have water depth around 20m, making them suitable locations for the wind turbine model used.

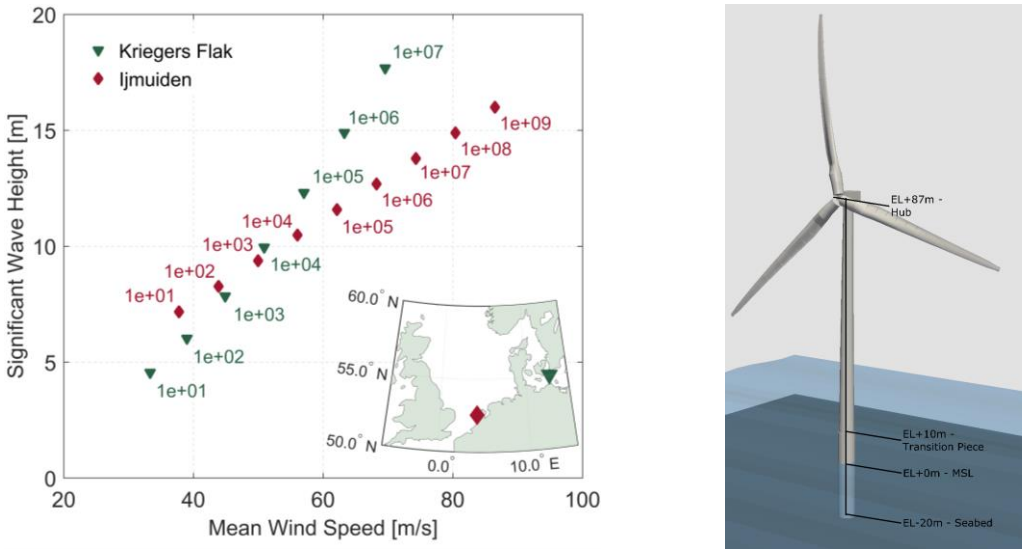

Figure 3: Comparison of the wind and wave conditions at different MRP for Krieger's Flak and Ijmuiden OWF sites (left), inset map shows site location. OWT structural model in FAST (right), main elevations highlighted.

2.3 Structural Model

The OWT considered in this study is based on the National Renewable Energy Laboratory (NREL) 5MW reference turbine [11], as shown on Figure 3 (right). A full list of dimensions and material properties are provided by Jonkman et al [11]. Dynamic response of the structure was calculated using the computer program FAST [12]. The turbulent wind profile across OWT was calculated externally using the program Turbsim [13], which generates turbulent wind histories for grid points covering the OWT by converting a Kaimal spectrum with turbulence type 'B' [14] into a stochastic time-history using Fast-Fourier transforms. The wave height time-history is generated by a similar process using the JONSWAP spectrum [10] then a 2nd order wave model to calculate water kinematics. The NREL 5MW turbine has a cut-off speed of $25m/s$, in all analysis the mean wind speed was above the cut-off and so DLC 6.1a [14] was used to select analysis parameters. However, as discussed above, we assess mean wind speeds well above the prescribed 50-year extreme MRP. The assumptions used in this study introduce a number of inaccuracies into the load-response calculation: firstly, no foundation is modelled. Secondly, the 2nd order wave model cannot capture the loads caused by large or breaking storm waves. However, the aim of this paper is to compare the relative properties of fragility curves dependant on different assumptions, therefore, the use of this simplified analysis is sufficient. Further studies are ongoing to investigate the impact of these assumptions.

2.4 Limit State Definition

The focus of this work is ULS failure of the OWT with failure occurring if either monopile or tower collapse we assess this using two different limit state calculations. The first is taken from the work of Sorenson et al [3] failure occurs when the tower plastic moment, subtracted by a factor calculated from the cross sectional properties, is reached, Eq. (1):

$$G_{Mcr} = \frac{1}{6}\left(1 - 0.84 \cdot \frac{D}{t} \cdot \frac{X_y F_y}{X_E E}\right)(D^3 - (D-2t)^3) X_y X_{cr} F_y - l_{ULT}(i, h_s, v_w) X_{dyn} X_{st} X_{ext} X_{sim} X_{exp} X_{aero} X_{str} \quad (1)$$

This will be referred to as the M_{cr} limit state for the remainder of the paper, $l_{ULT}(i, h_s, v_w)$ is the EDP and is defined as the maximum bending moment in structural analysis (i.e. a sample *i*-th) at a specific mean wind speed (v_w) and significant wave height (h_s). The X terms are variables which capture modelling uncertainty and are defined on Table 1. In Eq. (1), D is the component diameter, t is the thickness, F_y is the yield stress, and M_{cr} is the critical moment.

The NREL 5MW is a large utility scale OWT, therefore it has a low thickness to diameter ratio. Both the tower and monopile are non-compact according to the definition provided in DNV-OS-J101 Section 7.3.1 [15] and exceed the Eurocode Class 3 cross-section limits [16], this indicates potential shell behaviour. As a result the DNV steel buckling code [17] was used as the second limit state, which uses Von Mises stress as the EDP. The monopile buckling resistance ($f_{cap,M}(F_y, \sigma_{VM.M}(t))$) was calculated using the provisions for local shell buckling in Section 3.4 of [17]. The column buckling check was found to be unnecessary for the monopile, because it is fixed to the mudline which reduces its unconstrained length. The tower buckling resistance ($f_{cap,T}(F_y, \sigma_{VM.T}(t))$) was calculated using the provisions for column buckling in Section 3.8 of [17], which was found to be the most onerous provision. Both capacity variables are time-variant because the buckling strength is dependent on the stress state within the component, however it is demonstrated later, in Figure 6, that this variability is small. Structural demand is calculated by

transforming the force and moment outputs from FAST at each time step into stresses using a membrane shell calculation [17]. A single exceedance of the limit state was taken to result in failure of either component. The DNV limit state was also considered for both the tower (T) and monopile (M), Eq. (2):

$$G_{DNV,T} = f_{cap,T}\left(F_y, \sigma_{VM.T}(t)\right) \cdot X_y X_{cr} - \sigma_{VM.T}(t) \cdot X_{dyn} X_{st} X_{ext} X_{sim} X_{exp} X_{aero} X_{str}$$

$$G_{DNV,M} = f_{cap,M}\left(F_y, \sigma_{VM.M}(t)\right) \cdot X_y X_{cr} - \sigma_{VM.M}(t) \cdot X_{dyn} X_{st} X_{ext} X_{sim} X_{exp} X_{aero} X_{str} \quad (2)$$

The variables are the limit state function ($G_{DNV,T\ orM}$), tower Von Mises stress at each time step ($\sigma_{VM.T}(t)$), and monopile Von Mises stress at each time step ($\sigma_{VM.M}(t)$).
Random variables, shown on Table 1, were defined to capture the uncertainty in modelling the OWT. Variables associated with the structural properties were selected based on published data [3], [18]. Additionally, the environmental load model utilizes Fourier transforms to convert stationary frequency spectra into random time signals, in this context the random variable is the random phase angle used in the transform.

Table 1: Random variables associated with the structural model.

Type	Parameter	Mean	COV	Distribution
Structural	Structural Dynamics (X_{dyn})	1	0.05	Lognormal
	Aerofoil data uncertainty (X_{aero})	1	0.07	Gumbel
	Simulation statistics (X_{sim})	1	0.05	Normal
	Exposure (terrain) (X_{exp})	1	0.10	Normal
	Extrapolation (X_{ext})	1	0.05	Lognormal
	Climate statistics (X_{st})	1	0.05	Lognormal
	Stress evaluation (X_{str})	1	0.03	Lognormal
	Blade deflection model uncertainty ($X_{\delta l}$)	1	0.05	Lognormal
	Critical load capacity (X_{cr})	1	0.10	Lognormal
	Steel yield strength – MPa (F_y)	240	0.05	Lognormal
	Yield model uncertainty (X_y)	1	0.05	Lognormal
	Young's modulus model uncertainty (X_E)	1	0.02	Lognormal
Environmental	Wind Phase Angle	0	1	Uniform
	Wave Phase Angle	0	1	Uniform

2.5 Reliability Calculation

The probability of failure at different MRP can be estimated using the limit state function ($G_i = G_{Mcr}, G_{DNV,T}, G_{DNV,M}$). The plain Monte Carlo simulation estimator takes the form:

$$p_f(MRP_i) = P[G_i < 0 | IM = MRP_i] = \frac{1}{N_i}\sum_{k=1}^{N_i} I(G_{i,k} \leq 0) \quad (3)$$

Where N_i is the number of samples generated at each MRP and $I(G \leq 0)$ is an indicator function which takes the value 1 when the relevant limit state function is less negative.
Subset simulation is an efficient technique for simulating rare events, proposed by Au & Beck [7], based on splitting a rare event into a series of conditional probabilities which are easier to calculate. The probability of exceeding a threshold (b) is calculated iteratively by estimating the probability

of exceeding less rare thresholds $P(Y > b) = P(Y > b_i|Y > b_{i-1}) \subset \cdots \subset P(Y > b_1)$. The first subspace $P(Y > b_1)$ is calculated directly using Monte Carlo simulation and the samples that exceed the predefined limit (b_1) are used to define the limits of the conditional probability space $P(Y > b_2|Y > b_1)$. This procedure is repeated until the rare event threshold is met. Conditional samples are generated by using Metropolis algorithm Markov chains starting from point that exceeded the previous limit (b_{i-1}). Then the overall probability of a rare event occurring can be calculated by combining the initial and conditional probabilities:

$$P(Y > b) = P(Y > b_1) \prod_{i=2}^{m} P(Y > b_i|Y > b_{i-1}) \quad (4)$$

An algorithm based on subset simulation adaptively samples each input random variable. It simulates increasingly rare events until the point at which failure occurs (i.e. the limit state) is identified. The analyses summarised on Table 2 were run at each site, however, for brevity only the results from Krieger's Flak are presented as they are representative also of the Ijmuiden results. When material and modelling random variables were not used, the X terms in the limit state Eq. (1) and (2) were set to 1 and the yield strength to the mean value of $F_y = 240MPa$. To generate samples, N_i, multiple runs of the structural load calculation in FAST were generated for each MRP ($N_{MRP} = 16$) we generate 400 10-minute simulations, resulting in a total of 6400 individual analysis runs for each site.

Table 2: Summary of analyses

Analysis	Limit States	EDP Calculation	Random Variables	Reliability Calculation
1	DNV	Non-parameteric	No	Plain Monte Carlo
2	M_{cr}	Non-parameteric	No	Plain Monte Carlo
3	DNV + M_{cr}	Non-parameteric	Yes	Plain Monte Carlo
4	DNV + M_{cr}	Parameteric	Yes	Plain Monte Carlo
5	DNV + M_{cr}	Parameteric	Yes	Subset Simulation

3 Results

3.1 Analysis 1 - Influence of Analysis Length

The limit state Eq. (1) and (2) used in this work are both assumed to be time independent, an approach that has been widely used for assessing structural reliability under stochastic loading. However, the fundamental problem is time-dependant, i.e., there is a correlation between the maximum load experienced within a finite length simulation and the length of simulation. Converting wind and wave spectra into finite time series is naturally associated with a probability that we will not simulate the worst case combination of loading that could be generated by the spectra [19], with this probability linked to the analysis length. We justify using a time independent approach based on 10-minute long analyses by noting that the wind speeds measurements used are averaged over 10 minutes and that we assume the process of converting environmental spectra to time series accurately represents the actual physical process. Therefore, to capture the probability of exceeding a MRP based on 10-minute averaged measurements it is appropriate to use a 10-minute long simulation. In addition, we assume that the hazard component of the CAT modelling process, not considered here, will be based on 10-minute averages. There remains value in assessing the impact that

analysis length has on the properties of the fragility curve as a wide range of values, from 1.6 minutes [20] to 60 minutes [21] have been used in the literature.
Figure 4 compares fragility curves produced by selecting different averaging periods. Response at the longer analysis periods was calculated by combining the corresponding number of 10-minute simulations. The graphs indicate that the slope of the fragility curve and not just its location is sensitive to the analysis length, with longer analyses leading to a steeper fragility curves. This result demonstrates that the analysis period used to derive the fragility curve needs to be consistent with the hazard model otherwise bias will be introduced into the calculation of risk, which would comprise the later stages of the risk calculation.

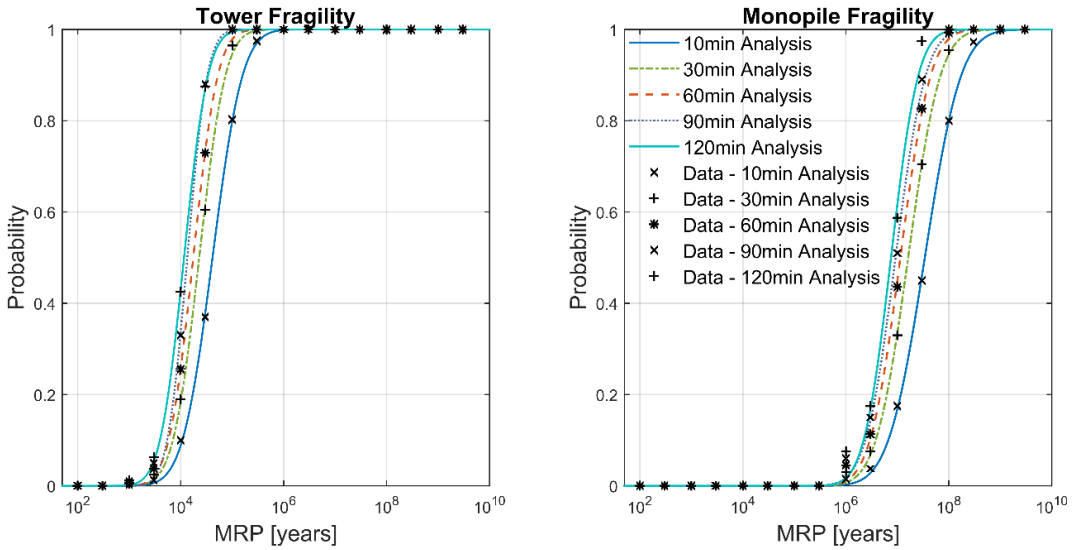

Figure 4: Comparisons of fragility curves produced for the tower and monopile of the NREL 5MW turbine at Krieger's Flak. The different curves indicate different analysis lengths.

3.2 Analysis 1-3 - Comparison of Limit States

The DNV and M_{cr} limit states are compared in Figure 5, the M_{cr} limit sate leads to failure at higher MRP than the DNV limit state. This effect occurs with both the tower and monopile, it can be explained by looking at the limit states in more detail. On Figure 6 (left) the moment capacity predicted using different limit states are compared; with the DNV limit state converted into an equivalent bending moment using a membrane stress calculation. The small variations in DNV capacity are caused when the Von Mises stress approaching 0 and affects the characteristic buckling stress. As discussed earlier, the M_{cr} limit state is calculated by subtracting a factor from the cross-section the plastic moment, for the NREL 5MW the reduction factor is approximately 0.1. Therefore, using the M_{cr} limit state, failure of the monopile will occur well above the point at which the outer fibre of the cross section first yields. On the other hand, the DNV local buckling limit state is calculated by dividing the yield stress by one plus the slenderness ratio to the power of 4, therefore it will always be less than the material yield stress. The column buckling limit state is based on a similar process of reducing the buckling strength. This explains why the fragility curve is shifted to the higher probability region when the DNV limit state is used.
Another useful comparison is to look at the effect of including additional random variables from Table 1 on the position and slope of the fragility curve. The results are also shown Figure 5 and demonstrate that, as expected, including random variables changes the slope of both limit state's fragility curves by a similar angle but has no impact on the location of the curve.

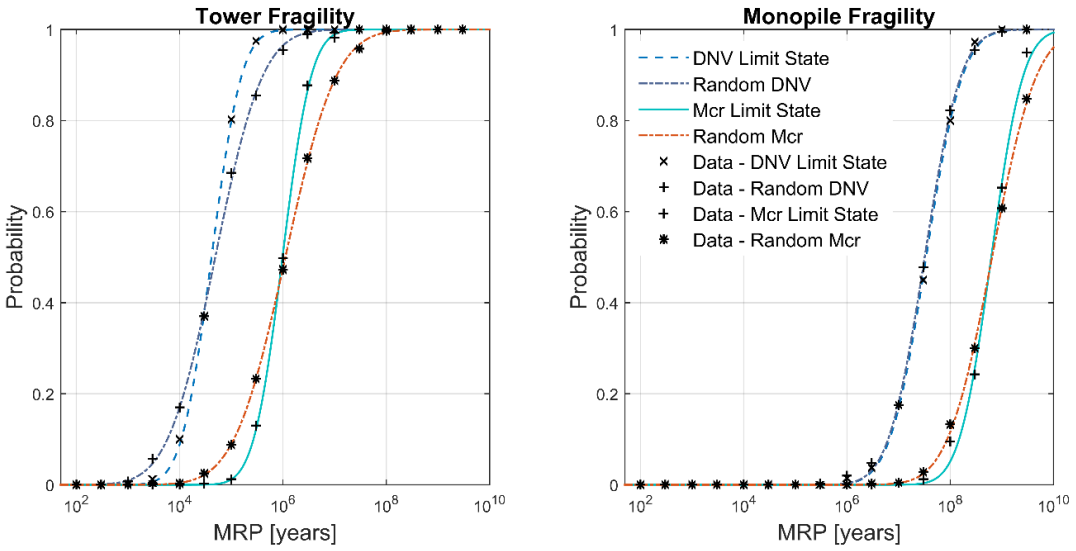

Figure 5: Comparisons of fragility curves produced for the tower and monopile of the NREL 5MW turbine at Krieger's Flak. The different curves indicate different limit states; all assessed using 10-minute length analyses.

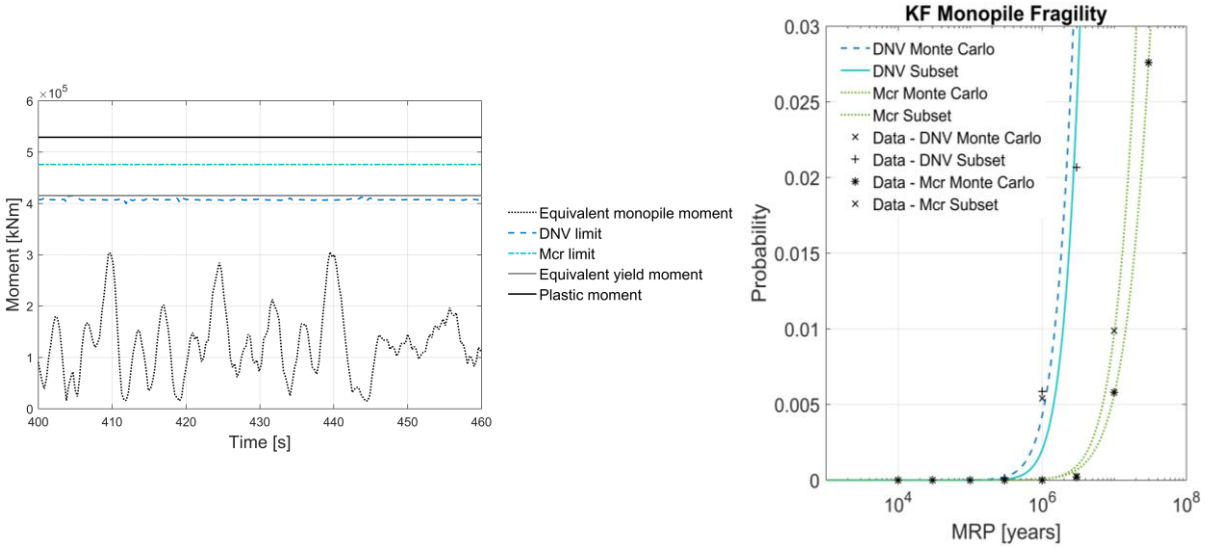

Figure 6: (left) Comparison between the limit states, all stresses converted into an equivalent bending moment. Graph is a segment of a full 600s time-history run at a MRP of $3 \cdot 10^7$*. (right) Comparisons of fragility curves produced for the monopile when subset simulation is used to improve lower tail fitting.*

3.3 Analysis 4 and 5 – Low Probability Fitting

The lower tail of the fragility curve was investigated in Analysis 4 and 5, using plain Monte Carlo and subset simulation. The general results computed for the monopile component are shown on Figure 6 (right). Details of the calculation for the M_{cr} limit state are representative of other limit states and are shown on Table 3. Subset simulation allowed the probability of failures to be calculated at the lower tail of the fragility curve, however for rare events the CoV in the probability of failure prediction grows large. In this analysis the EDP calculation involved sampling from a conditional distribution that had previously been fit to the output of FAST analyses, therefore the limit state could be solved without running a dynamic analysis. This meant a large number of samples could be generated, for Monte Carlo simulation we used 5000 samples and for the subset simulation algorithm we used step sized of 500 samples and a conditional probability step of 0.1. As the probability of failure increases in Table 3, the Monte Carlo technique appears to become more accurate than subset simulation and this is misleading: a constant number of samples were generated at each

MRP for plain Monte Carlo whereas for subset simulation the number of samples got progressively smaller (as less steps were required to find the failure region). The apparent increase in the accuracy of plain Monte Carlo simulation is therefore a result of the reducing sample size of the subset sample. The purpose of this comparison was to demonstrate the applicability of subset simulation to calculating the lower tail of a fragility curve as opposed to quantifying its accuracy. Subset simulation is useful if the lower tail of the fragility curve is of specific interest, however if estimating the general position of the curve is desired then Monte Carlo is easier to apply. In addition, care must be taken when simulating extremely rare events to avoid values of the random variables that are physically meaningless.

Table 3: Summary of analysis results at lower MRP at Krieger's Flak site for M_{cr} limit state.

MRP	P_f Monte Carlo	P_f Subset	CoV Monte Carlo	CoV Subset
1.00E+04	0	0	N/A	N/A
3.00E+04	0	2.60E-19	N/A	1.35
1.00E+05	0	4.54E-14	N/A	1.13
3.00E+05	0	6.64E-10	N/A	0.89
1.00E+06	0	1.58E-05	N/A	0.55
3.00E+06	0.0004	0.0005	0.71	0.41
1.00E+07	0.0052	0.0082	0.20	0.20
3.00E+07	0.0282	0.0366	0.09	0.14

4 Conclusions

Offshore wind farms play a key role in achieving the renewable energy targets for Europe (and worldwide) over the next decades. Europe is at the forefront of existing and planned offshore wind installations due to the rich wind resources. As the contribution to the overall electricity supply increases to significant levels, the resilience of the installed assets both in the short and long term needs to be assured. This paper represents a first step towards a novel, CAT risk- and resilience-based modelling approach for the asset management of offshore wind farms, taking both extreme weather conditions and structural fragility of the wind turbine system into account. In particular, the paper investigated the sensitivity of fragility functions to different modelling and analysis decisions, highlighting that:

1) Parametric approaches allow a large number of samples to be generated from using a smaller number of simulation calls, allowing the lower tail of the fragility curve to be investigated efficiently. It also allowed us to employ subset simulation to investigate more frequent but low probability of failure events which were unable to be investigated using non-parametric, plain Monte Carlo-based, simulations.
2) Both the limit state definition and the analysis length had a significant impact on the location of the fragility curve. Therefore, the choice of a limit state that accurately describes the problem being investigated is important. In particular, for a large diameter utility scale OWT the DNV limit state appears to be more suitable. It is conservative and includes the potential for local or column buckling structural components, both of which are plausible modes of failure given diameter to thickness ratios of OWT.
3) The hazard model should explicitly account for the impact of analysis length on the fragility, otherwise as demonstrated, bias will be introduced into the risk calculation due discrepancy between analysis length and environmental averaging period.

References

[1] "The European offshore wind industry - key trends and statistics 1st half 2016," 2016.

[2] P. Grossi and H. Kunreuther, Eds., *Catastrophe Modeling: A New Approach to Managing Risk*. Springer Science + Buisiness Media, 2005.

[3] J. D. Sorensen and H. S. Toft, "Probabilistic Design of Wind Turbines," *Energies*, vol. 3, no. 2, pp. 241–257, 2010.

[4] K. Wei, S. R. Arwade, A. T. Myers, S. Hallowell, J. F. Hajjar, E. M. Hines, and W. Pang, "Toward performance-based evaluation for offshore wind turbine jacket support structures," *Renew. Energy*, vol. 97, pp. 709–721, 2016.

[5] M. Mardfekri, "Multi-hazard reliability assessment of offshore wind turbines," Texas A&M University, 2012.

[6] K. Wei, S. R. Arwade, and A. T. Myers, "Incremental wind-wave analysis of the structural capacity of offshore wind turbine support structures under extreme loading," *Eng. Struct.*, vol. 79, pp. 58–69, 2014.

[7] S. K. Au and Y. Wang, *Engineering Risk Assessment with Subset Simulation*. John Wiley & Sons, 2014.

[8] T. Fischer, W. de Vries, and B. Schmidt, "Upwind Design Basis - WP4: Offshore Foudations and Support Structures," 2010.

[9] Niras A/S, "Kriegers Flak - MetOcean Report," 2014.

[10] DNV GL, *Environmental conditions and environmental loads*. 2010.

[11] J. Jonkman, S. Butterfield, W. Musial, and G. Scott, "Definition of a 5-MW reference wind turbine for offshore system development," *Contract*, no. February, pp. 1–75, 2009.

[12] B. Jonkman and J. Jonkman, "FAST Readme v8.12.00a-bjj," Denver, 2015.

[13] N. D. Kelley and B. Jonkman, "Overview of the TurbSim Stochastic Inflow Turbulence Simulator - NREL/TP-500-41137," 2007.

[14] IEC, "Wind turbines - Part 3: Design requirements for offshore wind turbines (IEC 61400-3-2009)."

[15] DNV GL, *Design of Offshore Wind Turbine Structures*. 2014.

[16] BSi, "Eurocode 3 - Design of steel structures - Part 1-1: General rules and rules for buildings - BS EN 1993-1-1:2005+A1:2014," 2005.

[17] DNV GL, *Buckling Strength of Shells*. 2013.

[18] N. J. Tarp-johansen, I. Kozine, L. Radermakers, J. D. Sørensen, and K. Ronold, *Optimised and Balanced Structural and System Reliability of Offshore Wind Turbines An account*, vol. 1420, no. April. 2005.

[19] D. Zwick and M. Muskulus, "The simulation error caused by input loading variability in offshore wind turbine structural analysis," *Wind Energy*, vol. 18, no. 8, pp. 1421–1432, 2015.

[20] A. Quilligan, A. O'Connor, V. Pakrashi, A. O'Connor, and V. Pakrashi, "Fragility analysis of steel and concrete wind turbine towers," *Eng. Struct.*, vol. 36, pp. 270–282, 2012.

[21] M. Muskulus and S. Schafhirt, "Reliability-based design of wind turbine support structures," in *Symposium on Reliability of Engineering Structures SRES'2015*, 2015, vol. 1, no. 1, pp. 12–22.